

**Partial-Wave Analysis of the  $\eta\pi^+\pi^-$  System Produced in the  
Reaction  $\pi^-p \rightarrow \eta\pi^+\pi^-n$  at 18 GeV/c**

J. J. Manak,<sup>\*</sup> T. Adams,<sup>†</sup> J. M. Bishop, N. M. Cason, E. I. Ivanov, J. M. LoSecco,  
A. H. Sanjari, W. D. Shephard, D. L. Stienike, S. A. Taegar,<sup>‡</sup> D. R. Thompson  
*Department of Physics, University of Notre Dame, Notre Dame, IN 46556, USA*

S. U. Chung, K. Danyo, R. W. Hackenburg, C. Olchanski, D. P. Weygand,<sup>\*</sup> H. J. Willutzki  
*Department of Physics, Brookhaven National Laboratory, Upton, NY 11973, USA*

A. R. Dzierba, J. Gunter, R. Lindenbusch, D. R. Rust, E. Scott, P. T. Smith, T. Sulanke,  
S. Teige  
*Department of Physics, Indiana University, Bloomington, IN 47405, USA*

S. P. Denisov, V. A. Dorofeev, I. A. Kachaev, V. V. Lipaev, A. V. Popov, D. I. Ryabchikov  
*Institute for High Energy Physics, Protvino, Russian Federation*

Z. Bar-Yam, J. P. Dowd, P. Eugenio,<sup>§</sup> M. Hayek,<sup>\*\*</sup> W. Kern, E. King, N. Shenhav<sup>\*\*</sup>  
*Department of Physics, University of Massachusetts Dartmouth, North Dartmouth, MA 02747,  
USA*

---

<sup>\*</sup>Present address: Thomas Jefferson National Accelerator Facility, Newport News, VA 23606, USA

<sup>†</sup>Present address: Department of Physics, Kansas State University, Manhattan, KS 66506, USA

<sup>‡</sup>Present address: Department of Physics, University of Arizona, Tucson, AZ 85721, USA

<sup>§</sup>Present address: Department of Physics, Carnegie Mellon University, Pittsburgh, PA 15213,  
USA

<sup>\*\*</sup>Permanent address: Rafael, Haifa, Israel

V. A. Bodyagin, O. L. Kodolova, V. L. Korotkikh, M. A. Kostin, A. I. Ostrovidov,  
L. I. Sarycheva, N. B. Sinev, I. N. Vardanyan, A. A. Yershov  
*Institute for Nuclear Physics, Moscow State University, Moscow, Russian Federation*

D. S. Brown,<sup>††</sup> T. K. Pedlar, K. K. Seth, J. Wise, D. Zhao  
*Department of Physics, Northwestern University, Evanston, IL 60208, USA*

G. S. Adams, J. P. Cummings, J. Kuhn, J. Napolitano, M. Nozar, J. A. Smith,  
D. B. White, M. Witkowski  
*Department of Physics, Rensselaer Polytechnic Institute, Troy, NY 12180, USA*

(E852 Collaboration)

(November 5, 2018)

## Abstract

A partial-wave analysis of 9082  $\eta\pi^+\pi^-n$  events produced in the reaction  $\pi^-p \rightarrow \eta\pi^+\pi^-n$  at 18.3 GeV/c has been carried out using data from experiment 852 at Brookhaven National Laboratory. The data are dominated by  $J^{PC} = 0^{-+}$  partial waves consistent with observation of the  $\eta(1295)$  and the  $\eta(1440)$ . The mass and width of the  $\eta(1295)$  were determined to be  $1282 \pm 5$  MeV and  $66 \pm 13$  MeV respectively while the  $\eta(1440)$  was observed with a mass of  $1404 \pm 6$  MeV and a width of  $80 \pm 21$  MeV. Other partial waves of importance include the  $1^{++}$  and the  $1^{+-}$  waves. Results of the partial wave analysis are combined with results of other experiments to estimate  $f_1(1285)$  branching fractions. These values are considerably different from

---

<sup>††</sup>Present address: Department of Physics, University of Maryland, College Park, MD 20742, USA

current values determined without the aid of amplitude analyses.

## I. INTRODUCTION

In this paper we present results of a partial-wave analysis of the  $\eta\pi^+\pi^-$  system in the 1210 to 1530 MeV/ $c^2$  mass region, as obtained from the study of the reaction

$$\pi^- p \rightarrow \eta\pi^+\pi^- n, \quad \eta \rightarrow 2\gamma \quad (1)$$

at 18.3 GeV/ $c$ . The data sample was collected during the summer of 1994 using the Multi-Particle Spectrometer (MPS) at the Alternating Gradient Synchrotron (AGS) facility of Brookhaven National Laboratory (BNL).

The identification of the isoscalar members of the  $J^{PC} = 0^{-+}$  and  $1^{++}$  nonets has been the subject of considerable interest, particularly with regard to searches for exotic mesons. It is known that such states often have  $a_0(980)\pi$  decay modes. Since the  $a_0(980)$  couples to both  $\eta\pi$  and to  $K\bar{K}$  final states, comparison of the resonances produced in the  $\eta\pi^+\pi^-$  and  $K\bar{K}\pi$  reactions can lead to important information with regard to this identification.

The  $\eta\pi^+\pi^-$  system is complicated, characterized by the large range of accessible quantum numbers ( $J^{PC} = 0^{-+}, 0^{--}, 1^{--}, 1^{+-}, 1^{++}, 2^{--} \dots$ ), a large number of possible  $\eta\pi$  and  $\pi\pi$  intermediate isobars ( $\sigma, \rho(770), a_0(980), f_2(1270), a_2(1320)$ )<sup>1</sup>, and the presence of overlapping resonances ( $f_1(1285), \eta(1295)$ ).

Historically, the low-mass region around the 1300 MeV/ $c^2$  enhancement in the  $\eta\pi^+\pi^-$  and  $K\bar{K}\pi$  mass spectra was called the D region. Most early analyses [1–6] made the assumption that a single state existed in this region in the presence of an incoherent (non-interfering) background. The problem was then the determination of the appropriate quantum numbers of this state and its branching ratio to  $\eta\pi^+\pi^-$ . Most early experiments showed a preference for  $J^{PC} = 1^{++}$  quantum numbers for this state, now referred to as the  $f_1(1285)$  [7].

Later, sufficiently high statistics were collected to carry out a partial wave analysis of the  $\eta\pi^+\pi^-$  system. Stanton *et al.* [8] performed an analysis of the reaction  $\pi^- p \rightarrow \eta\pi^+\pi^- n$

---

<sup>1</sup>We refer to the  $\pi\pi$  S-wave as  $\sigma$ . The form used for this is discussed in Section IV A.

at 8.45 GeV/c. The low-mass region was fit with a combination of  $0^{-+}$ ,  $1^{++}$ , and  $1^{+-}$  partial waves. Their analysis suggested the presence of a new state with  $J^{PC} = 0^{-+}$ , the  $\eta(1295)$ , as well as the  $f_1(1285)$ . In addition, it was suggested that the fit could be improved considerably if the  $0^{-+}$  partial waves were not allowed to interfere with the other waves in the fit.

The KEK-E179 collaboration performed two partial wave analyses [9,10] of the same reaction at 8 GeV/c. They too used a set of  $0^{-+}$ ,  $1^{++}$ , and  $1^{+-}$  partial waves to describe the low-mass region, and observed the  $f_1(1285)$  and  $\eta(1295)$ . Their analysis also suggested the presence of an additional state, now called [7] the  $\eta(1440)$ , in the high-mass region, which was earlier called the E region.

## II. APPARATUS

Figure 1 shows the elevation view of the experimental layout. The detector system consists of a charged-particle spectrometer and a downstream 3045-element lead-glass electromagnetic calorimeter (LGD) [11] [12] to provide neutral particle detection.

An 18.3 GeV/c  $\pi^-$  beam is incident on the 30-cm liquid-hydrogen target located at the center of the MPS magnet. Three threshold Čerenkov counters in the beam line are used to tag the beam particles as pions. Surrounding the target is a 198-element thallium-doped cesium iodide cylindrical veto array (CsI) [13] used in off-line analysis to reject events with wide-angle, low-energy photons from the decays of baryonic resonances. Between the target and the CsI is a four-plane cylindrical drift chamber (TCYL) [14] for triggering on recoil charged tracks. The downstream half of the magnet is equipped with three proportional wire chambers (TPX1-3) for triggering on forward charged-track multiplicity, and six drift chamber modules (DX1-6) for measuring the momentum of forward charged tracks. Also in the magnet is a window-frame lead-scintillator sandwich photon veto counter (DEA) which covers the solid-angle gap between the CsI and the LGD. Two scintillation counters are mounted on DEA, a window-frame counter (CPVC) to distinguish between charged and

neutral particles hitting DEA, and a rectangular counter (CPVB) which covers the hole in the DEA and is used, in conjunction with CPVC, to veto charged tracks in the all-neutral trigger. Beyond the magnet, and just upstream of the LGD, is a final drift chamber (TDX4) consisting of two X-planes, and two scintillation counters (BV and EV) for vetoing non-interacting beam particles and elastic-scattering events. Further details regarding the equipment are given elsewhere [15].

### III. DATA SELECTION AND PROPERTIES

The trigger for the  $\eta\pi^+\pi^-$  topology required a  $\hat{C}$ erenkov-tagged  $\pi^-$  incident on the target, two charged tracks emerging forward from the target, no charged recoil track, and an effective mass greater than that of the  $\pi^0$  in the LGD as determined by a hardware processor. Forty eight million triggers of this type were taken. From these, a final sample of events consistent with reaction 1 was selected by requiring:

- less than 20 MeV in the CsI to enhance recoil neutron events over  $N^*$  events;
- exactly two photons ( $\eta$ ) reconstructed in the LGD;
- a reconstructed beam track;
- two forward charged tracks of opposite charge;
- no recoil charged track;
- a 3-constraint SQUAW [16] kinematic fit to reaction 1 with a confidence level greater than 7%;
- $|t| < 3 \text{ GeV}^2/c^2$  after kinematic fitting, where  $t$  is defined as the magnitude of the four-momentum transfer squared between the target proton and the neutron in the final state.

The two-gamma mass distributions for about 10% of the data are shown before and after the above data selection cuts in Figs. 2(a) and (b) respectively. The  $\eta$  signal is nearly background free after cuts.

The  $\eta\pi^+\pi^-$  mass distribution for these events is shown in Figure 3. The  $\eta'(958)$  is evident. When fit with a Gaussian, a mass of  $961 \text{ MeV}/c^2$  with  $\sigma = 10 \text{ MeV}/c^2$  is obtained. This provides a measure of the mass resolution of the apparatus in the  $1000 \text{ MeV}/c^2$  mass region after kinematic fitting. An enhancement in the  $1300 \text{ MeV}/c^2$  region<sup>2</sup> is also observed, which, when fit to a Gaussian plus a linear background, yields a mass of  $1278 \text{ MeV}/c^2$  and  $\sigma = 20 \text{ MeV}/c^2$ .

In Figs. 4a, 4b and 4c we show the  $\eta\pi^-$ ,  $\eta\pi^+$  and  $\pi^+\pi^-$  effective mass distributions respectively for a three-body mass between  $1200$  and  $1540 \text{ MeV}/c^2$ . In Figs. 4a and 4b the  $a_0(980)$  peak is seen. The  $\rho(770)$  peak in Fig. 4c is cut off on the high-mass side because of the limited phase space available.

The same distributions are shown in Fig. 5(a)-(c) for the low mass subset of the data between  $1200$  and  $1350 \text{ MeV}/c^2$ . A very significant asymmetry between the  $\eta\pi^-$  and the  $\eta\pi^+$  distributions is evident. This asymmetry is due to the interference between  $I=0$   $a_0\pi$  and  $I=1$   $\rho\eta$  states, and is well-described in the partial-wave analysis described in the next section.

For the following analysis, 9,082 events were selected from the above data set in the region  $1205 \leq M(\eta\pi\pi) \leq 1535 \text{ MeV}/c^2$ .

#### IV. PARTIAL-WAVE ANALYSIS

---

<sup>2</sup>A detailed description of the Dalitz plot in this region is given elsewhere [15].

## A. Fitting Procedure

The formalism used in this analysis is based on the papers of Chung [17] and Chung and Trueman [18]. The analysis technique involved the use of the reflectivity basis to describe the individual partial waves and the maximization of an extended log likelihood function in the fitting procedure. Fits are carried out independently in each  $\eta\pi^+\pi^-$  mass bin. The procedure and analysis programs are described by Cummings and Weygand [19].

Due to the large number of possible partial waves accessible to the  $\eta\pi^+\pi^-$  system, a complete analysis requiring all possible isobars and partial waves is not practical given the limited statistics. In principle one would like to include all possible isobars:  $\sigma, \rho, a_0, f_2, a_2$  and a large set of partial waves ( $J < 4$ ). Because this analysis is limited to the low-mass region, we can neglect the  $a_2$  and the  $f_2$  isobars.<sup>3</sup> Furthermore, we choose to consider only amplitudes with  $J < 2$  since there are no known states with higher spin in this low-mass region which decay into  $\eta\pi\pi$ .

An incoherent isotropic background was included in some trial fits, but it was not used in the final fit. This type of background is, except for the  $\pi\pi$  mass dependence of the amplitude, similar to a non-interfering  $J = 0, \sigma\eta$  partial wave, making them quite difficult to differentiate.

In order to determine whether both spin-flip and non-flip amplitudes at the baryon vertex are required to fit the data, fits were attempted for both rank 1 and 2. (If both types of amplitudes are not necessary, the rank 1 fit will give a good description of the data.) The likelihood function was improved greatly when the fit rank was increased to two. In addition, rank 1 fits to the data were found to become unstable in the absence of a background wave. We conclude that a rank 2 fit is required to fit the data; rank 1 fits were not used.

The  $\rho$  isobar was modeled by a relativistic Breit-Wigner amplitude with parameters

---

<sup>3</sup> The  $f_2(1270)$  could in principle reach this final state through the  $a_2\pi$  mode, but this is highly suppressed by phase space.



extracted from the Particle Data Book [7]. For the final fit the  $a_0$  isobar was modeled as a Breit-Wigner form with a mass of  $980 \text{ MeV}/c^2$  and a width of  $72 \text{ MeV}/c^2$  [15]. The  $\pi\pi$  S-wave (the  $\sigma$ ) was represented by a parameterization of the  $\pi^+\pi^-$  S-wave provided by K. L. Au *et al.* [20]. Alternate parameterizations of the  $a_0$  and the  $\sigma$  were explored [21]. However it was found that the particular choice of parameterization had little effect on the final results.

To determine the appropriate waves for the  $1200\text{-}1350 \text{ MeV}/c^2$  region, a fit was performed using a coarse bin width of  $50 \text{ MeV}/c^2$  with all waves with  $J < 2$  included. Waves were then discarded from the fit if their removal had little effect on the value of the likelihood function ( $|\Delta\mathcal{L}| < 5$ ). Selected waves were then re-introduced in the fit to insure the stability of the solution. In total, several hundred different sets of partial waves were fit. For each combination of partial waves, the binning,  $t$  cuts, and starting values of the fit parameters were varied to insure stability of the final solution. The set of waves chosen for the final fit is shown in Table I.

For the final fit, a bin width of  $30 \text{ MeV}/c^2$  was chosen. This was a compromise between achieving adequate statistics in each mass bin and acquiring the best possible resolution in the entire mass region  $1200\text{-}1540 \text{ MeV}/c^2$ . The starting values of the fit were randomly chosen and the entire spectrum was re-fit several times to insure stability with the finer bin width. For bin widths smaller than  $30 \text{ MeV}/c^2$  the fits often became unstable, converging to different solutions depending upon the starting values.

It is interesting to note that the final waves selected for the low-mass region are consistent with those used by Stanton *et al.* [8] and by Fukui *et al.* [9]. The only exception is that we do not use a  $1^{+-} a_0\pi$  wave. While the inclusion of this wave in the fit for the low-mass region is reasonable, providing a natural explanation for the odd-even isospin interference observed in the data, we found that the fit could not distinguish this wave from the  $1^{+-} \rho\eta$  wave in this mass range. Due to the unambiguous presence of the  $\rho\eta$  partial wave at higher mass, it was decided not to include the  $1^{+-} a_0\pi$  partial wave in the final set.

## B. Results of Partial Wave Analysis

### 1. $J^{PC} = 0^{-+}$ Partial Waves

The fitted intensity distribution for the  $0^{-+}$   $a_0\pi$  wave as a function of  $\eta\pi^+\pi^-$  effective mass is shown in Fig. 6a. A sharp peak at  $\approx 1300$  MeV/ $c^2$  is evident, consistent with the observation of  $\eta(1295) \rightarrow a_0\pi$ . Some intensity is seen extending out to 1400 MeV/ $c^2$ . It should be noted that the majority of the signal for this wave comes from the second rank of the fit. This indicates a different production mechanism than that for the  $1^{+-}$  and the  $1^{++}$  waves (which are produced dominantly in the first rank) and means that these latter waves do not interfere with the  $0^{-+}$  wave (see discussion below).

As shown in Fig. 6b, the  $0^{-+}\sigma\eta$  wave is double-peaked, with structure suggestive of  $\eta(1295)$  and  $\eta(1440)$  production. The dominant nature of the structure seen in the high-mass region in this wave is somewhat inconsistent with previous analyses [9,10] which observe the presence of a  $\sigma\eta$  decay of the  $\eta(1440)$ , but do not see it as dominant.

A large fraction of the  $0^{-+}$  signal occurs in the second rank, especially for the  $\sigma\eta$  partial waves in the high-mass region. Because these waves do not interfere with the other dominant waves in the fit, reliable relative phase motion could not be obtained.

The  $a_0\pi$  and  $\sigma\eta$   $0^{-+}$  waves were added coherently in each rank and then summed incoherently. The result is shown in Fig. 6c. The  $\eta(1295)$  and  $\eta(1440)$  peaks are clearly visible. The spectrum was fit with two spin-0 Breit-Wigner forms plus a quadratic background. Fitted values of the masses and widths are given in Table II. In addition, the  $a_0\pi/\sigma\eta$  branching ratio were determined from Fig. 6 for both the  $\eta(1295)$  and the  $\eta(1440)$ . These values are also given in Table II.

### 2. $J^{PC} = 1^{++}$ Partial Waves

In Fig. 7a the  $1^{++}$   $a_0\pi$  partial wave intensity distribution is shown. This wave shows evidence for the  $f_1(1285)$ . The amount of  $f_1$  signal is comparable to the  $0^{-+}$  signal in the

$a_0\pi$  channel. No significant structure is observed at higher mass.

In Fig. 7b the  $1^{++} \sigma\eta$  partial wave intensity distribution is shown. This wave does not show any structure, but was necessary to the fit for bins above  $1450 \text{ MeV}/c^2$ .

In Fig. 7c the coherent sum of the  $1^{++}$  partial waves is shown. This sum displays a peak in the vicinity of the  $f_1(1285)$  and a rise at high mass. A comparison of Fig. 7c and Fig. 6c reveals that the majority of the signal strength in the  $1200\text{-}1500 \text{ MeV}/c^2$  mass region arises not from  $1^{++}$  partial waves, but from the  $0^{-+}$  wave. This observation is especially important for the low-mass region because several previous analyses [2,6] for branching ratio estimates assumed that the low-mass region was dominated by the  $1^{++}$  wave. We find that the ratio of the  $1^{++}$  intensity to the sum of the  $1^{++}$  and  $0^{-+}$  intensities in the region  $1235\text{-}1325 \text{ MeV}/c^2$  is  $0.19 \pm 0.06$ .

The observed  $f_1(1285)$  signal in Fig. 7c is in the same mass region with a very similar width as the  $\eta(1295)$ . To eliminate the possibility that this  $1^{++}$  ( $f_1$ ) signal is an artifact, due to “leakage” from the larger  $0^{-+}$  ( $\eta$ ) signal, a Monte-Carlo study was performed. The measured amplitudes, with the contribution due to the  $1^{++}$  wave removed, were used to generate Monte-Carlo events taking into account the experimental resolution, acceptance and statistics. These events were then analyzed in exactly the same manner as the data. The resulting  $1^{++}$  intensity in the low-mass region was found to be less than 2% of the total signal, and consistent with zero. This leads to the conclusion that the observed signals are not artifacts of the analysis or apparatus, and are, in fact, two distinct resonances.

### 3. $\rho\eta$ Partial Waves

The intensity distribution for the  $1^{+-} \rho\eta$  wave is shown in Fig. 8a. This wave was seen in all previous analyses and is significant in the low-mass region. Previous experiments [9] have claimed this wave to show evidence for production of the  $b_1(1235)$  with a  $\rho\eta$  decay mode. However, we do not observe any structure in the  $1^{+-}$  wave to support this conjecture. As mentioned earlier, this wave is, nevertheless, essential for producing the  $a_0^+/a_0^-$  asymmetry

observed in the data.

In Fig. 8b the  $1^- \rho \eta$  intensity distribution is shown. This is the only negative-reflectivity partial wave in our analysis, and it does not interfere with any other partial waves in the fit. The wave steadily increases throughout the low-mass region, consistent with its being the low-mass tail of the  $\rho(1700)$ .

## V. DISCUSSION OF THE $f_1(1285)$ BRANCHING FRACTIONS

Production of the  $\eta(1295)$  dominates the low-mass peak, accounting for roughly 80% of the signal. This observation has implications on the  $f_1 \rightarrow \eta\pi\pi$  branching fraction. Previous experiments [1,2,5,6] have determined the  $f_1 \rightarrow \eta\pi\pi$  branching fraction without the aid of a partial wave analysis under the assumption that the low-mass peak consists of a single  $f_1$  state resting on top of an incoherent background. This assumption is clearly incorrect, and values for the earlier determinations of the branching fractions need to be corrected.

Corden *et al.* [2] studied the reactions  $\pi^- p \rightarrow \eta\pi^+\pi^- n$  and  $\pi^- p \rightarrow K\bar{K}\pi n$  at 15 GeV/c. In their analysis they obtained a  $K\bar{K}\pi/\eta\pi\pi$  branching ratio in the low-mass region of  $0.5 \pm 0.2$  without the aid of a partial wave analysis. It is reasonable to assume that the relative production of  $f_1(1285)$  and  $\eta(1295)$  is the same in the present experiment as in that of Ref. [2] since the experiments are close in energy and study the same final state. It is also reasonable to assume that the  $K\bar{K}\pi$  decay at low mass is entirely due to  $f_1(1285)$  decay since this conclusion was reached by a partial wave analysis [22] of the data. Thus the  $K\bar{K}\pi/\eta\pi\pi$  branching ratio of the  $f_1(1285)$ , as quoted by Corden *et al.*, should be corrected by dividing it by the fraction of the low-mass peak which is due to  $f_1(1285)$  decay. We thus obtain  $(0.5 \pm 0.2)/(0.19 \pm 0.06) = 2.6 \pm 1.4$  for this branching ratio.

We can perform the same type of estimate using, instead of our own analysis, the results of KEK-E179 [9] for the reaction  $\pi^- p \rightarrow \eta\pi^+\pi^- n$  at 8.95 GeV/c. In that experiment, the fraction of the low-mass peak which is due to  $f_1(1285)$  decay is claimed to be 50%. Again, using the results of Corden *et al.* (although in this case the difference in the energies of the

experiments is larger), we obtain an alternate estimate of the  $K\bar{K}\pi/\eta\pi\pi$  branching ratio for  $f_1$  decay to be  $1.0 \pm 0.4$ .

We can estimate the effect which these results can have on the  $f_1(1285)$  branching fractions by assuming that the low-mass signal observed in the  $K\bar{K}\pi$ ,  $\gamma\rho^0$ , and  $4\pi$  decay modes is due only to  $f_1(1285)$  decay. This is the most reasonable for the  $K\bar{K}\pi$  mode as mentioned above because the other two decay modes ( $\gamma\rho^0$ ,  $4\pi$ ) have not been as thoroughly investigated.<sup>4</sup> Nevertheless, using the PDG98 branching ratios [7] of  $0.271 \pm 0.016$  for  $K\bar{K}\pi/4\pi$  and  $0.45 \pm 0.18$  for  $\gamma\rho^0/2\pi^+2\pi^-$ , the  $f_1(1285)$  branching fractions can be calculated. (We also assume the branching ratio for  $4\pi/2\pi^+2\pi^- = 3$  as in [7].) In Table III we list the  $f_1(1285)$  branching fractions derived by the above procedure.

Assigning systematic errors to these  $f_1(1285)$  branching fractions is difficult because of the undetermined uncertainties in branching ratios for the  $4\pi$  and  $\gamma\rho^0$  decay modes. However, it is clear from the above exercise that the results from the present experiment and the KEK experiment for the  $f_1(1285)$  branching fractions are consistent, and those listed in the particle data book [7] need to be corrected. The most significant result is the large reduction in the  $f_1 \rightarrow \eta\pi\pi$  branching fraction.

## VI. SUMMARY AND CONCLUSIONS

A partial wave analysis was performed on 9082  $\eta\pi^+\pi^-n$  events in the  $1205 \leq M(\eta\pi^+\pi^-) \leq 1535$  MeV/ $c^2$  mass interval. The analysis used a rank 2 fit with 30 MeV/ $c^2$  bins and a set of 6 partial waves. The partial waves used in the fit were:  $0^{-+}a_0\pi$ ,  $0^{-+}\sigma\eta$ ,  $1^{+-}\rho\eta$ ,  $1^{++}a_0\pi$ ,  $1^{++}\sigma\eta$  and  $1^{--}\rho\eta$ .

The low-mass region was found to include a large contribution from the  $0^{-+}$  wave which indicates the production of  $\eta(1295)$ . Evidence of  $f_1(1285)$  production was seen in the  $1^{++}$

---

<sup>4</sup>Of these modes the  $4\pi$  branching fraction is most suspect due to the large number of interfering partial waves which contribute to a  $4\pi$  data set.

wave. The fact that the region is dominated by  $\eta(1295)$  production leads to significant changes in the  $f_1(1285)$  branching fractions as discussed in Section V.

The  $\eta(1295)$  was seen to decay to both  $a_0\pi$  and  $\sigma\eta$ . The  $a_0\pi/\sigma\eta$  branching ratio for  $\eta(1295)$  was estimated to be  $0.48 \pm 0.22$ . The mass and width of the  $\eta(1295)$  were determined to be  $1282 \pm 5 \text{ MeV}/c^2$  and  $66 \pm 13 \text{ MeV}/c^2$  respectively. This result is consistent with the PDG98 summary of  $\eta(1295)$  mass and width of  $1297 \pm 2.8 \text{ MeV}/c^2$  and  $53 \pm 6 \text{ MeV}/c^2$ , respectively.

The high-mass region is dominated by a large  $0^{-+}\sigma\eta$  signal present in the second rank of the fit. This signal is consistent with production of a single state, the  $\eta(1440)$ . The mass and width of the  $\eta(1440)$  are estimated to be  $1404 \pm 6 \text{ MeV}/c^2$  and  $80 \pm 21 \text{ MeV}/c^2$ . This result is consistent with the PDG98 [7] weighted average value for the mass and width of the  $\eta(1440)$  determined from the  $\eta\pi\pi$  mode of  $1405 \pm 5 \text{ MeV}/c^2$  and  $56 \pm 7 \text{ MeV}/c^2$ , respectively.

The  $\eta(1440)$  has been previously observed in the reaction  $\pi^-p \rightarrow K\bar{K}\pi n$ , in  $p\bar{p}$  annihilation, and in the radiative decay of  $J/\psi$ , with decays in the  $a_0\pi$  and  $K\bar{K}^*$  modes. Studies of the  $\pi^-p \rightarrow \eta\pi^+\pi^-n$  reaction have yielded both a  $\sigma\eta$  and an  $a_0\pi$  component of the  $\eta(1440)$ . In the present analysis, it is found that the  $\sigma\eta$  decay dominates, while the KEK analyses [9,10] suggest a larger  $a_0\pi$  component. The estimate of the  $a_0\pi/\sigma\eta$  branching ratio for  $\eta(1440)$  from the present analysis is  $0.15 \pm 0.04$ . The systematic errors are unassigned, but assumed to be large due to the difficulty of the fit in distinguishing  $0^{-+}a_0\pi$  and  $0^{-+}\sigma\eta$  waves from each other.

In addition to the  $f_1(1285)$ ,  $\eta(1295)$  and the  $\eta(1440)$  contributions, a large, relatively structureless signal in the  $1^{+-}\rho\eta$  wave was observed throughout the low mass region. This wave has also been observed in all previous partial wave analyses of the  $\pi^-p \rightarrow \eta\pi^+\pi^-n$  system. There is no obvious resonance interpretation of this structure, but its presence is required to account for the large  $a_0^+/a_0^-$  production asymmetry seen in the low mass region. A  $1^{--}\rho\eta$  partial wave, consistent with the low-mass tail of the  $\rho(1700)$ , is also seen.

We would like to express our deep appreciation to the members of the MPS group. Without their outstanding efforts, the results presented here could not have been obtained.

We would also like to acknowledge the invaluable assistance of the staffs of the AGS and BNL, and of the various collaborating institutions. This research was supported in part by the National Science Foundation and the US Department of Energy.

TABLES

TABLE I. Partial Waves Used in Final Fit

<i>I</i> <i>sospin</i>	$J^{PC}$	Isobar	$l$	$m$	$\epsilon$
1	$1^{--}$	$\rho$	1	0	-1
0	$0^{-+}$	$a_0$	0	0	+1
0	$0^{-+}$	$\sigma$	0	0	+1
0	$1^{++}$	$a_0$	1	0	+1
0	$1^{++}$	$\sigma$	1	0	+1
1	$1^{+-}$	$\rho$	0	0	+1

TABLE II. Properties of the  $J^{PC} = 0^{-+}$  States

	Mass (GeV/ $c^2$ )	Width (GeV/ $c^2$ )	$a_0\pi/\sigma\eta$ Branching Ratio
$\eta(1295)$	$1.282 \pm 0.005$	$0.066 \pm 0.013$	$0.48 \pm 0.22$
$\eta(1440)$	$1.404 \pm 0.006$	$0.080 \pm 0.021$	$0.15 \pm 0.04$

TABLE III.  $f_1$  Branching Fractions

Decay Mode	PDG [7]	BNL-E852	KEK-E179 [9,10]
$4\pi$	$35 \pm 4\%$	$65 \pm 4\%$	$59 \pm 5\%$
$\eta\pi\pi$	$50 \pm 18\%$	$7 \pm 3\%$	$16 \pm 5\%$
$\gamma\rho^0$	$5.4 \pm 1.2\%$	$10 \pm 4\%$	$9 \pm 3\%$
$K\bar{K}\pi$	$9.6 \pm 1.2\%$	$18 \pm 1\%$	$16 \pm 1\%$



## REFERENCES

- [1] J. H. Campbell *et al.*, Phys. Rev. Lett. **22**, 1204 (1969).
- [2] M. J. Corden *et al.*, Nucl. Phys. **B144**, 153 (1978).
- [3] O. I. Dahl *et al.*, Phys. Rev. **164**, 1377 (1967).
- [4] R. Nacasch *et al.*, Nucl. Phys. **B203**, 203 (1978).
- [5] C. Defoix *et al.*, Nucl. Phys. **B44**, 125 (1972).
- [6] A. Gurtu *et al.*, Nucl. Phys. **B151**, 181 (1979).
- [7] Particle Data Group: C. Caso *et al.*, The European Physical Journal **C3**, 1 (1998).
- [8] N. R. Stanton *et al.*, Phys. Rev. Lett. **42**, 346 (1979).
- [9] S. Fukui *et al.*, Phys. Rev. B **267**, 293 (1991).
- [10] A. Ando *et al.*, Phys. Rev. Lett. **57**, 1296 (1986).
- [11] B. Brabson *et al.*, Nucl. Instr. & Meth A **332**, 419 (1993).
- [12] R. R. Crittenden, Nucl. Instr. & Meth A, **387**, 377 (1997).
- [13] T. Adams *et al.*, Nucl. Instr. & Meth A **386**, 617 (1996).
- [14] Z. Bar-Yam *et al.*, Nucl. Instr. & Meth A **342**, 398 (1994).
- [15] S. Teige *et al.*, Phys. Rev. **D59**, 012001 (1999).
- [16] O. I. Dahl *et al.*, “SQUAW kinematic fitting program”, Univ. of California, Berkeley Group A programming note P-126, unpublished (1968).
- [17] S.U. Chung, “Formulas for Partial-Wave Analysis”, Brookhaven BNL-QGS-93-05, unpublished (1993).
- [18] S.U. Chung and T.L. Trueman, Phys. Rev. D **111**, 633 (1975).

- [19] J. P. Cummings and D. P. Weygand, “The New BNL Partial Wave Analysis Programs”, BNL-64637, unpublished (1997).
- [20] K. L. Au *et al.*, Phys. Rev. D **35**, 1633 (1986).
- [21] C. Amsler *et al.*, Phys. Lett. B **335**, 425 (1995).
- [22] A. Birman *et al.*, Phys. Rev. Lett. **61**, 1557 (1988).

FIGURES  
E852 APPARATUS LAYOUT

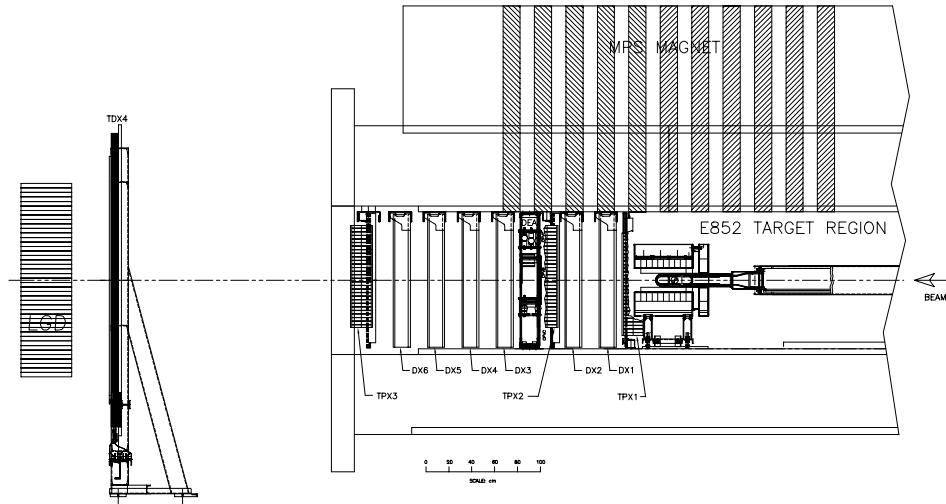


FIG. 1. E852 Apparatus Layout

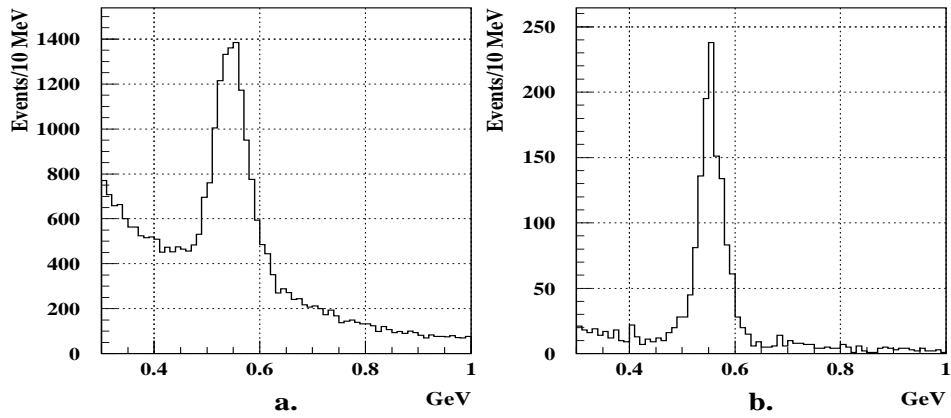


FIG. 2. Two  $\gamma$  invariant mass distribution (a) before cuts, (b) after data selection cuts.

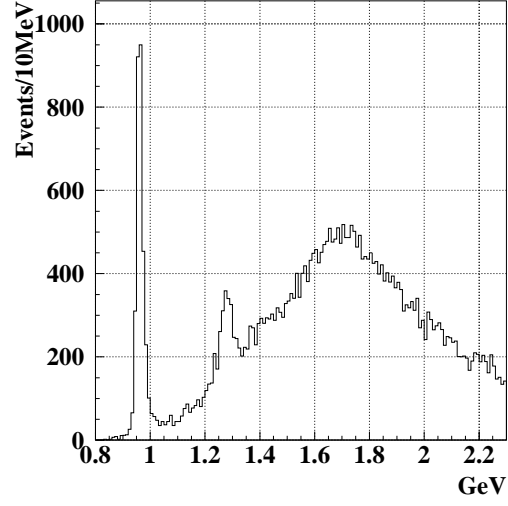


FIG. 3.  $\eta\pi^+\pi^-$  three-body mass distribution (not corrected for acceptance).

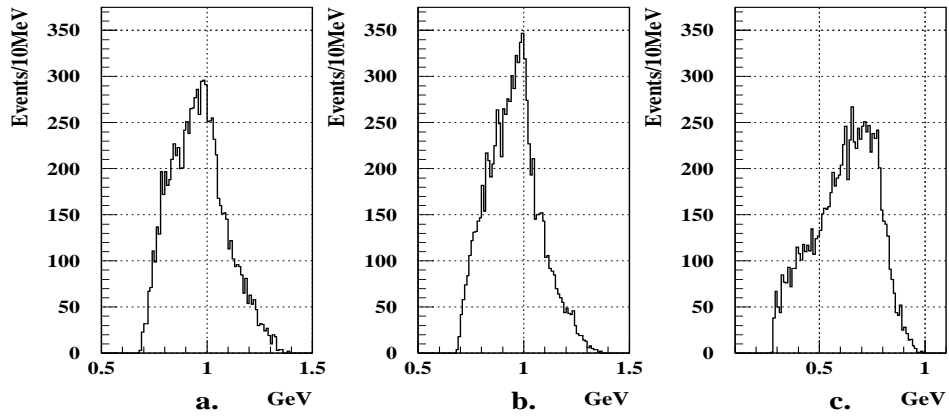


FIG. 4. Two-body mass distributions: a)  $\eta\pi^-$  b)  $\eta\pi^+$  and c)  $\pi^+\pi^-$  for the  $\eta\pi^+\pi^-$  mass region between 1200 and 1540  $\text{MeV}/c^2$ .

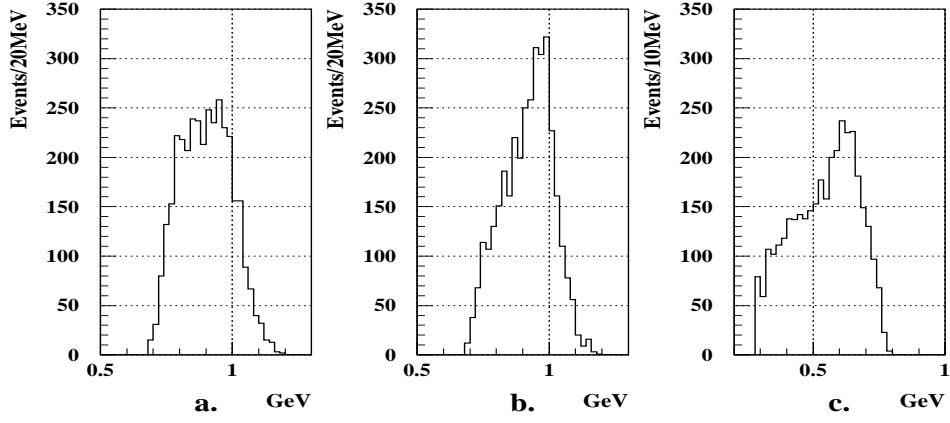


FIG. 5. Two-body mass distributions: a)  $\eta\pi^-$  b)  $\eta\pi^+$  and c)  $\pi^+\pi^-$  for the  $\eta\pi^+\pi^-$  mass region between 1200 and 1350  $\text{MeV}/c^2$ .

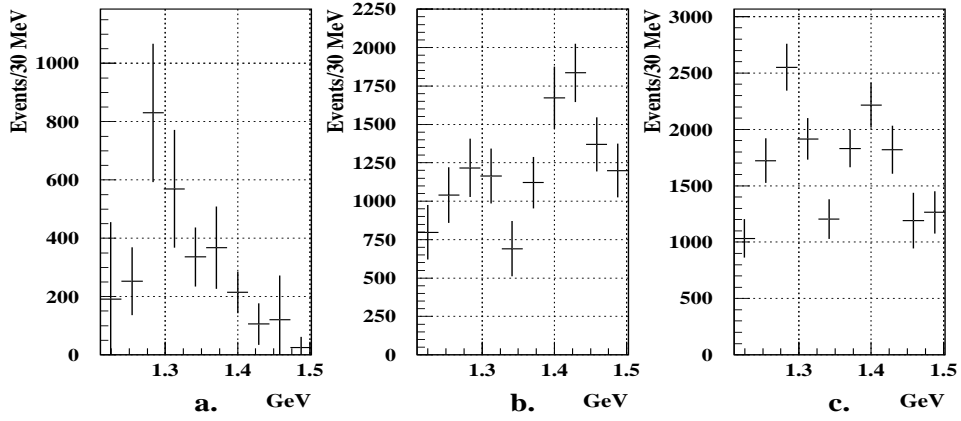


FIG. 6. a:  $0^{-+}a_0\pi$  intensity, b:  $0^{-+}\sigma\eta$  intensity, c: Total  $0^{-+}$  intensity

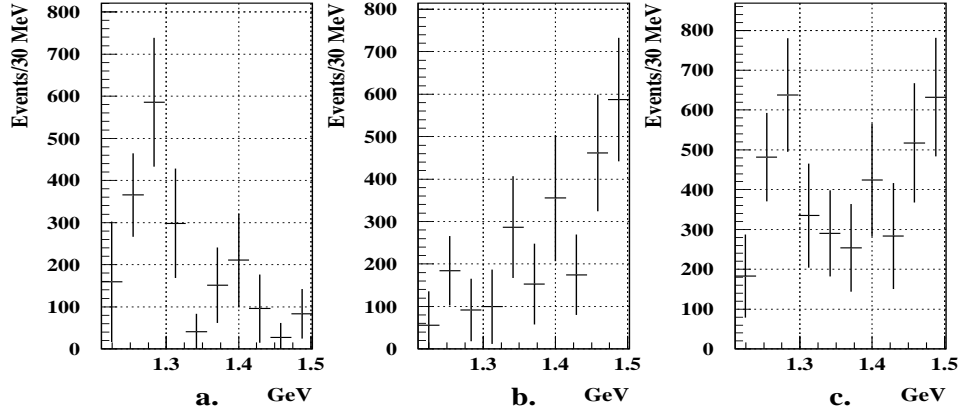


FIG. 7. a:  $1^{++} a_0 \pi$  intensity, b:  $1^{++} \sigma \eta$  intensity, c: Total  $1^{++}$  intensity

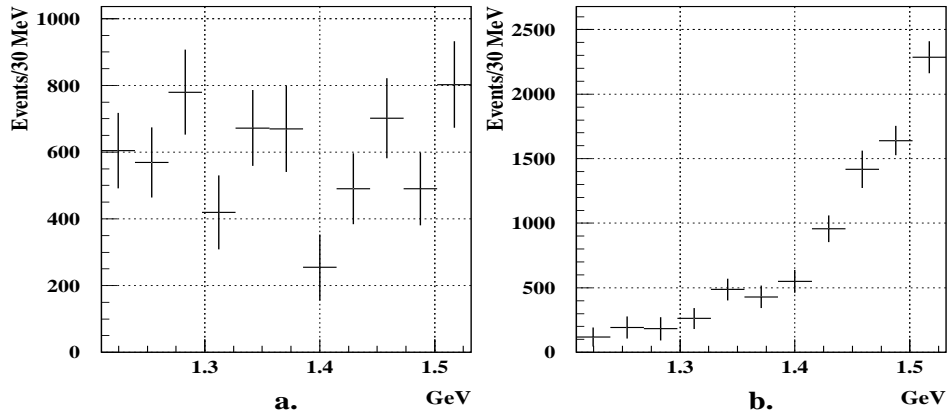


FIG. 8. a:  $1^{+-} \rho \eta$  intensity, b:  $1^{- -} \rho \eta$  intensity (negative reflectivity partial wave)